ACS OMEGA

Article

Cite This: ACS Omega 2019, 4, 9284−9293

http://pubs.acs.org/journal/acsodf

A Composite of Hyaluronic Acid-Modified Graphene Oxide and Iron Oxide Nanoparticles for Targeted Drug Delivery and Magnetothermal Therapy

Nilkamal Pramanik,[†,‡] Santhalakshmi Ranganathan,[‡] Sunaina Rao,[‡] Kaushik Suneet,[†] Shilpee Jain,[†] Annapoorni Rangarajan,[†,‡] and Siddharth Jhunjhunwala*[,†]

[†]Centre for BioSystems Science and Engineering and [‡]Molecular Reproduction, Development and Genetics, Indian Institute of Science, Bengaluru 560012, India

Supporting Information

ABSTRACT: Graphene oxide (GO) nanoparticles have been developed for a variety of biomedical applications as a number of different therapeutic modalities may be added onto them. Here, we report the development and testing of such a multifunctional GO nanoparticle platform that contains a grafted cell-targeting functionality, active pharmaceutical ingredients, and particulates that enable the use of magnetothermal therapy. Specifically, we demonstrate the ability to covalently attach hyaluronic acid (HA) onto GO, and the resultant nanoparticulates (GO-HA) exhibited low inherent toxicity toward two different breast cancer cell lines, BT-474 and MDA-MB-231. Doxorubicin (Dox) and paclitaxel (Ptx) were successfully loaded onto GO-HA with high and moderate efficiencies, respectively. A GO-HA-Dox/Ptx system was significantly better than the GO-Dox/Ptx system at specifically killing CD44-expressing MDA-MB-231 cells but not BT-474 cells that do not express CD44. Further, modified iron oxide nanoparticles were loaded onto the GO-HA-Dox system, enabling the use of magnetic hyperthermia. Hyperthermia in combination with Dox treatment through the GO-HA system showed significantly better performance in reducing viable tumor cell numbers when compared to the individual systems. In summary, we showcase a multifunctional GO nanoparticle system that demonstrates improved efficacy in killing tumor cells.

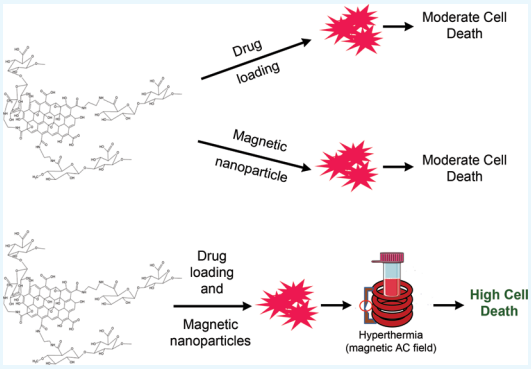

INTRODUCTION

Graphene oxide (GO)-based nanomaterials have shown tremendous promise in controlled delivery of therapeutic agents.[1−3] The unique physicochemical properties of GO such as its large surface area, its ability to interact with and adsorb hydrophobic molecules, and its relative inertness to biological substances make it an ideal choice as a base material for drug delivery.[1,4,5] A number of drug delivery systems utilizing GO are being developed, and a significant majority of these systems focus on their use for delivering chemotherapeutics.[4,5] However, like many other systems, GO-based delivery of chemotherapeutics suffers from the inability to target specific cells in the body. This may be overcome by the attachment of targeting moieties on GO.

A molecule that may be used for targeted delivery of chemotherapeutics is hyaluronic acid (HA).[6] HA is a naturally occurring polysaccharide that is present in the extracellular matrix where it plays an important role in promoting structural integrity of tissues and mediates cell attachment. HA is able to function in this manner as many cell surface proteins (receptors) bind to it, and CD44 is one such receptor, which is highly expressed on certain types of tumor cells.[7] Utilizing the CD44-binding capacity of HA, many reports have shown the efficacy of GO modified with HA for targeted delivery of chemotherapeutic agents.[8−10] However, the GO-HA chemotherapeutic system does have its limitations. Modified versions of these systems using molecules that enable photothermal[11−14] or magnetothermal[15] therapy have been developed also, but individually, many of them do not appear to be potent enough for killing all tumor cells.

To overcome this issue, here, we explore the use of GO as a base material to prepare a composite with multiple functionalities. We hypothesized that a composite that combines numerous functionalities into the same system is likely to be significantly better at killing the vast majority of tumor cells. To test this hypothesis, we developed a GO-based system that is capable of targeting specific cells (through HA conjugation) and delivering chemotherapeutic agents (through doxorubicin or paclitaxel loading) and may be used for magnetothermal therapy (through addition of iron oxide nanoparticles[16−19]). We perform thorough chemical characterization of the prepared nanocomposites and show their efficacy in targeted killing of a

Received: March 29, 2019
Accepted: May 15, 2019
Published: May 28, 2019

DOI: 10.1021/acsomega.9b00870
ACS Omega 2019, 4, 9284−9293

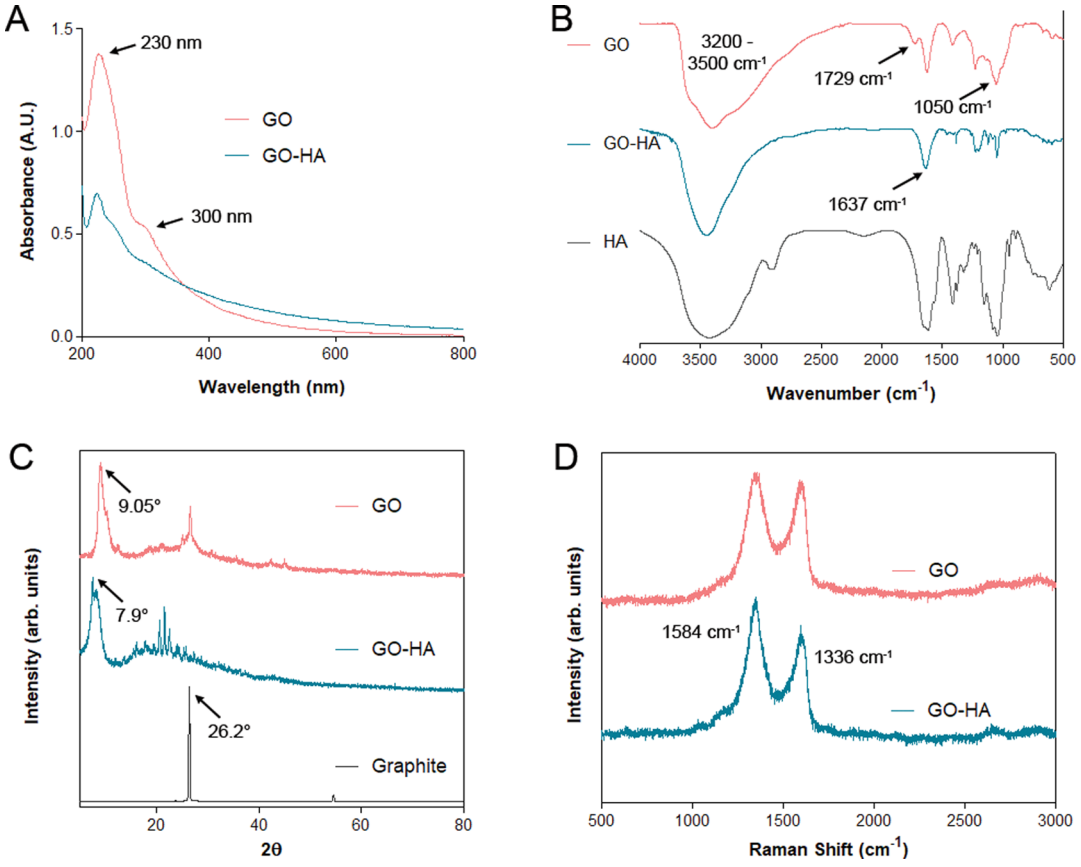

Figure 1. Characterizations of GO and GO-HA. (A) UV−visible spectroscopic measurements, (B) FTIR spectroscopy, (C) X-ray diffraction analysis, and (D) Raman spectroscopic analysis, with characteristic peaks highlighted.

breast cancer cell line overexpressing CD44. Further, we demonstrate that brief exposures to AC magnetic fields (AMF) in combination with chemotherapeutic loaded on to the nanocomposite result in improved antitumor efficacy.

RESULTS AND DISCUSSION

Material Characterization. First, to confirm the syntheses of graphene oxide (GO) and hyaluronic acid-modified GO (GO-HA), UV−visible, X-ray diffraction (XRD), FTIR, and Raman spectroscopic analyses were performed. UV−visible spectroscopy analyses (Figure 1A) of both GO and GO-HA show absorbance peaks around 230 nm and a shoulder at 300 nm, which correspond to $\pi-\pi^*$ and $n-\pi^*$ transitions,[20] respectively. The FTIR spectra (Figure 1B) showing the presence of −OH (3200−3500 cm^{-1}), C═O (1729 cm^{-1}), and C−O (1050−1060 cm^{-1}) demonstrate the synthesis of GO. Additionally, the GO-HA FTIR spectra exhibited an absence of the 1729 cm^{-1} peak (C═O) and a strong 1637 cm^{-1} peak suggestive of an amide bond. For GO, XRD (Figure 1C) showed a shift in the peak from 26.2° (graphite) to 9.05° and a d_{001} value of 0.97 nm, indicating the incorporation of different functional groups that resulted in exfoliation of graphite layers. GO-HA showed a slight increase in the d-spacing value to 1.13 nm, peak shift to 7.9°, and additional peaks in the range of 15°−30° (2θ). Raman spectroscopic analysis of GO[21] (Figure 1D) revealed the strong absorption peaks at 1336 cm^{-1} (D-band) and 1584 cm^{-1} (G-band). Additionally, the D/G ratio was measured to be 1.04, suggesting the introduction of disorder into the graphene sheets as a result of oxidation, which was further increased for GO-HA. Overall, the characterization data shows the successful synthesis of GO, and subtle differences in the characterization data of GO-HA when compared to GO are suggestive of the incorporation of HA onto GO.

To further verify the incorporation of HA onto GO, X-ray photoelectron spectroscopy (XPS) was performed. XPS analysis of GO (Figure 2) revealed significant peaks between 284 and 289 eV (C1s spectrum) and a broad peak around 535 eV (O1s spectrum) attributed to the presence of C−C, C═C, C−O−C, C═O, O—C═O, O═C, O−C, and O—C═O groups.[22,23] In the case of GO-HA (Figure 2), the C1s and O1s spectra showed similar peaks. In addition, the presence of peaks in the N1s spectrum was observed, specifically 399.1 and 400.5 eV, which correspond to the secondary amine and amide groups, respectively,[24] confirming the successful formation of an amide linkage, which would occur only if HA was incorporated onto GO.

Particulate Characterization. Next, dynamic light scattering and atomic force microscopy were performed to characterize the size, charge, and surface morphology of the graphene oxide particulates. The hydrodynamic size of the particulate suspensions also provides information on their stability in aqueous solutions. Dynamic light scattering measurements showed that GO and GO-HA had similar hydrodynamic diameters of 184.1 ± 33.1 and 166.8 ± 16.2 nm, respectively. The particulates were negatively charged as would be expected for oxides of graphene, with zeta potential values of −18 ± 3.2 mV (GO) and −21.5 ± 2.25 mV (GO-HA). Particulate sizes as determined by atomic force microscopy (Figure 3) showed slightly lower lateral dimensions (130−160 nm) as would be expected for dried particles. Additionally, the calculated

DOI: 10.1021/acsomega.9b00870
ACS Omega 2019, 4, 9284−9293

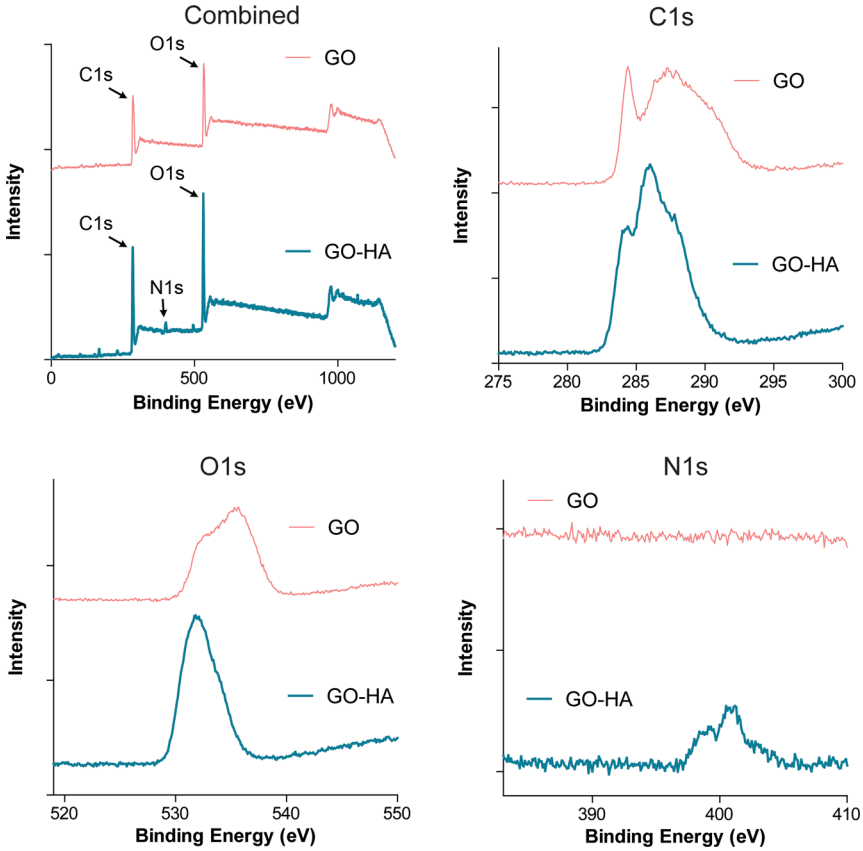

Figure 2. X-ray photoelectron spectroscopy of GO and GO-HA. Characteristic C1s and O1s peaks were observed in both nanoparticulates, but an N1s peak was observed only in GO-HA, which confirms the presence of nitrogen-containing chemical groups associated with HA.

thickness of the graphene oxide sheets was measured to be between 1 and 2.5 nm for both GO and GO-HA, confirming that these were nanosized particulates. Further, transmission electron micrographs of GO showed the exfoliated wave-like monolayer or bilayers graphene sheets, while GO-HA exhibited a network-like geometry (Supplementary Figure 1).

Doxorubicin (Dox) Loading and Release. Dox was loaded onto the graphene oxide particulates by simple mixing. Based on the aromatic character of both graphene oxide sheets and Dox, loading was expected to occur through adsorption. Dox loading on graphene oxide particulates was confirmed through UV−visible and FITR spectroscopies (Supplementary Figure 2). Loading efficiency (amount of drug loaded to the initial amount added) was calculated to be 86.0 ± 10.7% for GO and 87.0 ± 5.6% for GO-HA. The high loading efficiency is likely a result of the large surface area on graphene oxides, the aromatic $\pi-\pi$ interaction, and possibly hydrogen bonding interaction between the amine group on Dox and hydroxyl/carboxylic groups of graphene oxide. In terms of weight percentage of the final complex (ratio of mass of drug to mass of particulate + drug), the calculated amounts were 33.2 ± 2.8% for GO and 33.5 ± 1.4% for GO-HA.

To investigate the release kinetics of the drug from graphene oxides, in vitro release studies were performed in buffers of two different pH values: pH 7.4 (extracellular) and pH 5.5 (endosomal inside the cell). Figure 4 shows the kinetics of release from GO and GO-HA. At physiological pH, Dox release from both GO and GO-HA exhibited an initial burst followed by slow release over a period of 48 h. Under conditions of lower pH (5.5), a higher burst followed by potentially faster rates of release was observed from both particulates, with 53 and 61% of loaded drug released over a period of 48 h. The higher burst release in an acidic environment could possibly be due to lowered hydrogen bonding between the amine group of DOX molecules and the hydroxyl group of graphene oxide nanoparticles. These results suggest that, in extracellular spaces (or in the blood), a limited amount of drug would be released from these particulates, and a larger portion of the drug would release only upon the intracellular uptake of the nanoparticulates.

In Vitro Cytocompatibility. Next, intrinsic cytocompatibilities of GO and GO-HA was investigated using two cell lines: MDA-MB-231 (a hyaluronic receptor CD44-expressing cell line) and BT-474 (cell line with negligible expression of CD44).[25] Cultures of these cell lines with nanoparticulates show that, at low concentrations of particulates (≤25 μg/mL), live cell numbers were close to those of control (absence of particulates) cultures (Figure 5A,B). At higher concentrations (100 μg/mL), both particulates were found to result in 25−35% reduction in live cell numbers, which could be a result of particulate-associated toxicity or due to reduced cell growth in the presence of the particulates. In the case of the MDA-MB-231 cell line, two-way ANOVA showed that significant differences in cell viability are found at higher concentrations. Importantly, significant differences were not observed between the cytocompatibilities of GO and GO-HA (two-way ANOVA, source of variation as treatment), suggesting that they were similarly compatible at all concentrations. Further, at lower concentrations of particulates, the compatibilities of particulates on both cell lines were also similar. For all further studies, we used graphene oxide particulates at ≤10 μg/mL concentrations.

DOI: 10.1021/acsomega.9b00870
ACS Omega 2019, 4, 9284−9293

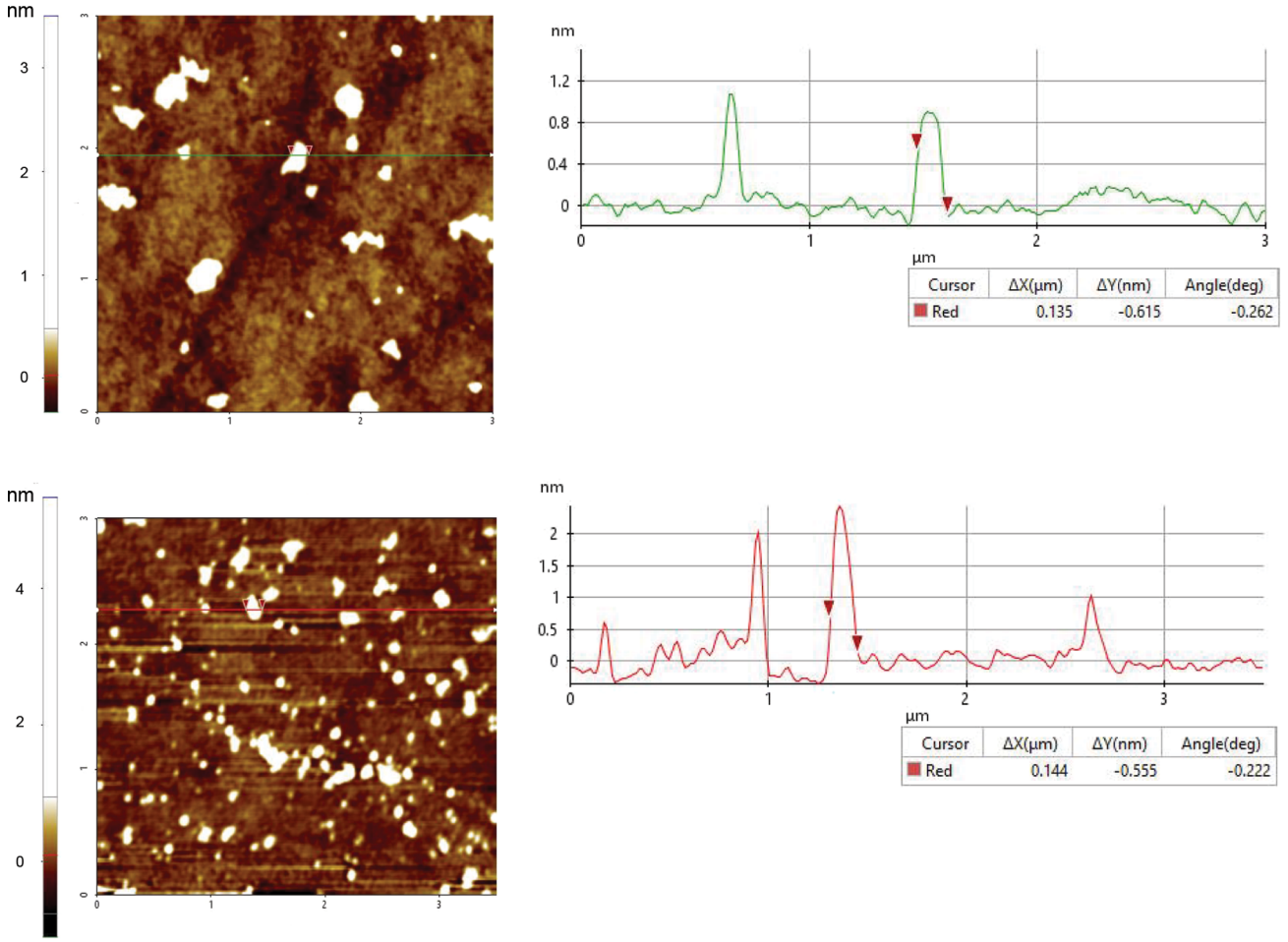

Figure 3. Atomic force microscopy of GO (top) and GO-HA (bottom). Representative scans of GO and GO-HA are shown on the left. On the right side are line profiles that indicate the lateral dimensions (ΔX) of the particulates (measured to be between 130 and 160 nm) and enable the calculation of thickness.

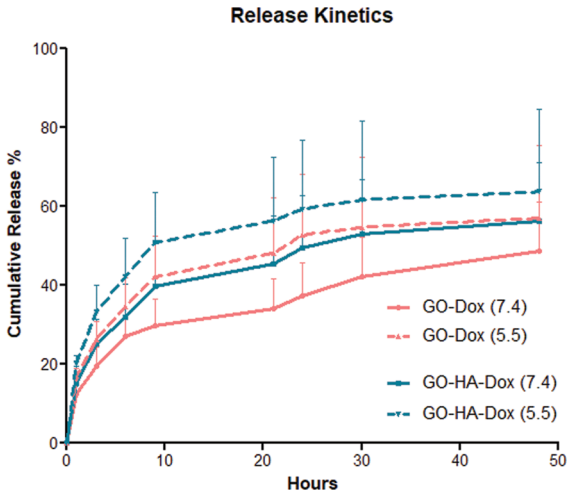

Figure 4. Release kinetics of Dox from nanoparticulates. Releases from both GO-Dox and GO-HA-Dox systems were measured in buffers of two different pH values. Data is based on $n = 3$ independent release measurements at each time point.

Cytotoxicity of Dox-Loaded GO and GO-HA Particulates. The therapeutic efficacy of the nanoparticulates was evaluated by loading Dox on them and testing their ability to improve killing of tumor cells in vitro. For these studies, Dox (in its dispersed form) was used as a control, and equivalent amounts of Dox loaded on particulates were tested. When tested on BT-474 cells, no differences in cell viability were observed between GO-Dox and GO-HA-Dox (Figure 6A). However, when tested on MDA-MB-231 (CD44-expressing cells), GO-HA was found to be significantly better at reducing the number of viable cells when compared to GO at high concentrations (Figure 6B). This difference is likely due to HA conjugation, which is thought to improve the interaction and uptake of GO-HA into cells. Another interesting aspect of the observed result is that the targeting feature enables much higher efficacies to specific cells. That is, while Dox is effective at killing both cells and GO-Dox is not as effective in killing either cell type, GO-HA-Dox is much more effective at killing CD44-expressing cells while not as effective at killing CD44-negative cells. We suggest that this difference could be a result of improved uptake of GO-HA when compared to GO particulates, as shown in Supplementary Figure 3. Hence, the HA-conjugated system is likely to be more effective on target cells and has lower side effects on nontarget cells.

Paclitaxel (Ptx)-Loaded System. One of the major advantages of the graphene oxide particulates is that they may be used as the platform technology on which a number of features may be added. In place of Dox (or in combination with it), another chemotherapeutic may be used. Here, we show that Ptx may be loaded onto graphene oxide particulates in a similar

DOI: 10.1021/acsomega.9b00870
ACS Omega 2019, 4, 9284−9293

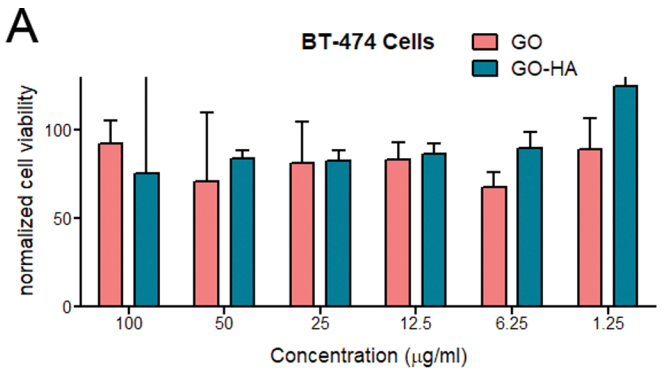

Two-way ANOVA (BT-474)

Source of Variation	P value summary
Interaction	ns
Concentration	ns
Treatment (GO vs GO-HA)	ns

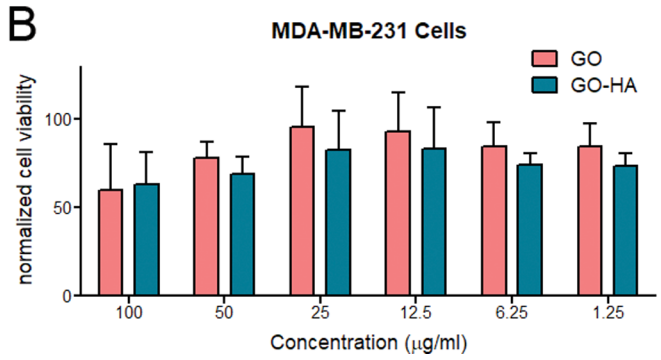

Two-way ANOVA (MDA-MB-231)

Source of Variation	P value summary
Interaction	ns
Concentration	** ($p < 0.01$)
Treatment (GO vs GO-HA)	ns

Figure 5. Cytocompatibilities of nanoparticulates. Varying concentrations of particulates were cultured with (A) BT-474 and (B) MDA-MB-231, and their effect on cell viability was determined. Cell viability measurements are normalized to control cultures of cells in the absence of any particulates. Statistical testing was performed using two-way ANOVA, and the results are displayed in tables adjacent to the graphs.

manner (Supplementary Figure 4). Loading efficiencies were measured to be 30.8 ± 9.6% for GO and 34.0 ± 11.6% for GO-HA, and weight percentages were 23.1 ± 1.7% for GO and 28.1 ± 7.0% for GO-HA. These Ptx-loaded graphene oxide particulates were also effective at reducing the number of viable CD44-expressing MDA-MB-231 cells, possibly by blocking tubulin-mediated cell division.[26] Also, as observed for the Dox system, the GO-HA-Ptx nanoparticulates were significantly better than the GO-Ptx, again suggestive of targeted delivery (Figure 7).

Composite of Graphene Oxide and Iron Oxide Particulates. In both drug-loaded GO-HA systems, it was observed that the lowest normalized cell viability was around 30%, suggesting that all tumor cells were not killed. To improve the killing efficacy, another feature that may be added to the graphene oxide particulates is their ability to be used for magnetothermal therapy. Along these lines, we synthesized iron oxide particles and loaded them onto the graphene oxide particulates (Supplementary Figure 5). With the help of these iron oxide particles, the temperature around the composite particulates may be raised using magnetic fields, and such magnetothermal therapies may be used to enhance the efficacy of chemotherapeutics in killing tumor cells.[19] The vibrating sample magnetometer (VSM) analysis of the composite system exhibited a small hysteresis loop (Supplementary Figure 6A) having a saturation magnetic moment (M_s) value of 46.68 emu/g. Placing our composite system in AC magnetic fields resulted in an increase in temperature, as would be expected (Supplementary Figure 6B). Next, the efficacy of such a system in killing MDA-MB-231 (CD44 expressing) tumor cells was determined by first incubating the composite particulates with cells, followed by a brief (10 min) exposure of this entire system to magnetic fields for 10 min, followed by incubation for 48 h. While the magnetic hyperthermia alone resulted in a non-significant reduction in the number of viable cells (Figure 8A), the combination of hyperthermia and drug (Dox loaded on the nanoparticulates) was significantly better at reducing the number of viable cells when compared to use of drug only (Figure 8B). These results suggest that the GO-HA system may be effectively used to develop composites for combination therapies, and more specifically, the combination of targeting followed by hyperthermia along with chemotherapeutic treatment results in significantly greater killing of tumor cells (in this case, cells expressing CD44) with less harm to other cells (in this case, cells not expressing CD44).

Breakdown of Graphene Oxide Particulates. Finally, it has been suggested that graphene oxide nanoparticulates may be degraded in the body by immune cells.[27−29] To assess if the particulates prepared herein behave similarly, GO and GO-HA were incubated for 24 h with a macrophage cell line and then analyzed using Raman spectroscopy. As reported by others in cultures with neutrophils or neutrophil enzymes, a decrease in the D-band and G-band was observed in the case of RAW cell-incubated GO and GO-HA (Supplementary Figure 7). Breakdown of GO-HA appears to be less than GO in this timeframe, which may be due to the presence of chemical groups that affect enzymatic activity, as suggested by Kurapati et al.[30]

CONCLUSIONS

In summary, we demonstrate the successful synthesis of graphene oxide particulates and show that they may be used as a platform for the addition of multiple functionalities. First, we demonstrate that hyaluronic acid may be grafted onto GO, and chemotherapeutic drugs may be loaded onto these particles to

DOI: 10.1021/acsomega.9b00870
ACS Omega 2019, 4, 9284−9293

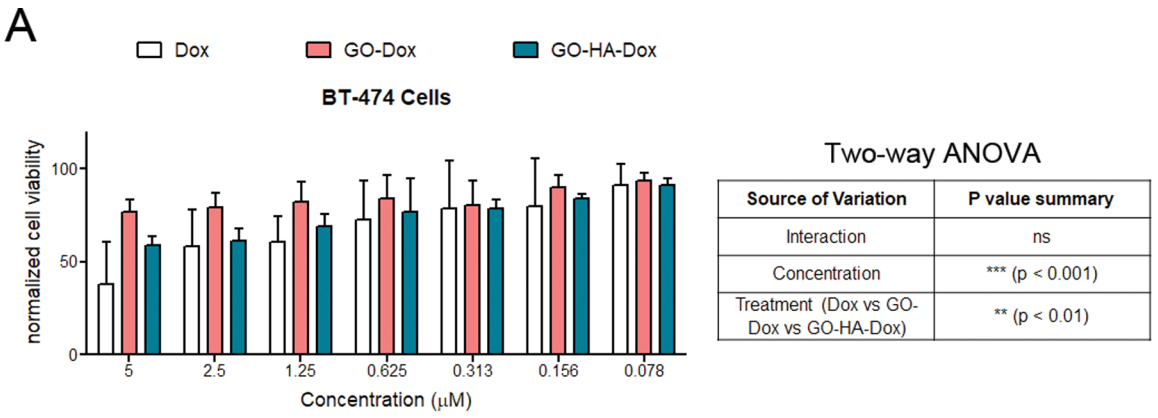

Two-way ANOVA

Source of Variation	P value summary
Interaction	ns
Concentration	*** (p < 0.001)
Treatment (Dox vs GO-Dox vs GO-HA-Dox)	** (p < 0.01)

Bonferroni post-tests

Dox vs. GO-Dox

Concentration (μM)	P value
5	* - P < 0.05
2.5	P > 0.05
1.25	P > 0.05
0.625	P > 0.05
0.313	P > 0.05
0.156	P > 0.05
0.078	P > 0.05

Dox vs. GO-HA-Dox

Concentration (μM)	P value
5	P > 0.05
2.5	P > 0.05
1.25	P > 0.05
0.625	P > 0.05
0.313	P > 0.05
0.156	P > 0.05
0.078	P > 0.05

GO-Dox vs. GO-HA-Dox

Concentration (μM)	P value
5	P > 0.05
2.5	P > 0.05
1.25	P > 0.05
0.625	P > 0.05
0.313	P > 0.05
0.156	P > 0.05
0.078	P > 0.05

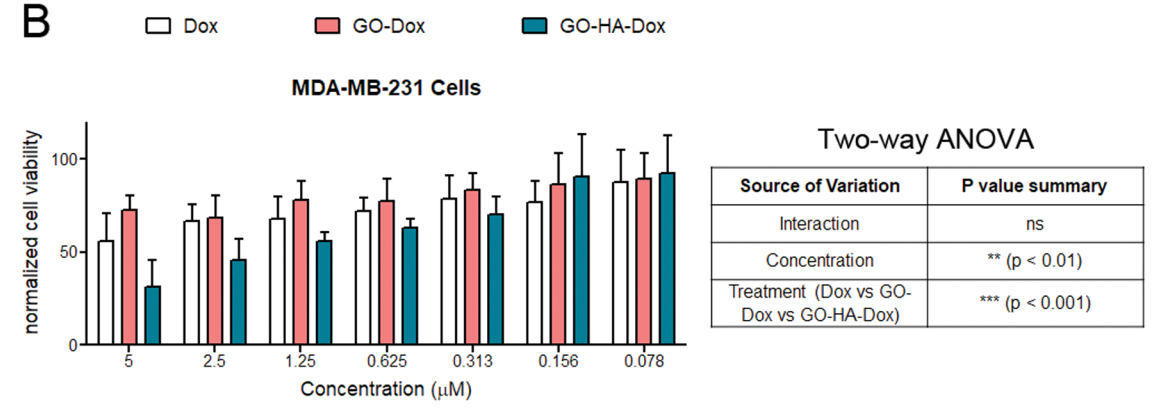

Two-way ANOVA

Source of Variation	P value summary
Interaction	ns
Concentration	** (p < 0.01)
Treatment (Dox vs GO-Dox vs GO-HA-Dox)	*** (p < 0.001)

Bonferroni post-tests

Dox vs. GO-Dox

Concentration (μM)	P value
5	P > 0.05
2.5	P > 0.05
1.25	P > 0.05
0.625	P > 0.05
0.313	P > 0.05
0.156	P > 0.05
0.078	P > 0.05

Dox vs. GO-HA-Dox

Concentration (μM)	P value
5	P > 0.05
2.5	P > 0.05
1.25	P > 0.05
0.625	P > 0.05
0.313	P > 0.05
0.156	P > 0.05
0.078	P > 0.05

GO-Dox vs. GO-HA-Dox

Concentration (μM)	P value
5	*** - P < 0.001
2.5	P > 0.05
1.25	P > 0.05
0.625	P > 0.05
0.313	P > 0.05
0.156	P > 0.05
0.078	P > 0.05

Figure 6. Cytotoxicity of Dox-loaded nanoparticulates. Varying concentrations of Dox (either in a suspension form or on particulates) were added to two different breast cancer cell lines, (A) BT-474 and (B) MDA-MB-231, and their effect on cell viability was determined. Cell viability measurements are normalized to control cultures of cells in the absence of any Dox or particulates. Statistical analysis of data (two-way ANOVA) was performed, and significant differences were observed, which are reported in tables associated with the graphs.

enable killing of tumor cells. Next, we show that the addition of a magnetothermal functionality using iron oxide nanoparticles loaded onto the GO-HA-drug system results in significantly improved killing efficacy when compared to systems with only one functionality. These composite particulates with targeting, chemotherapeutic, and magnetothermal functionalities have the

DOI: 10.1021/acsomega.9b00870
ACS Omega 2019, 4, 9284−9293

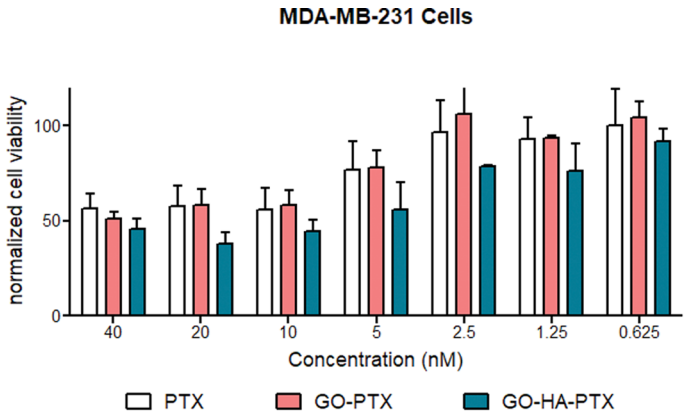

Two-way ANOVA

Source of Variation	P value summary
Interaction	ns
Concentration	*** (p < 0.001)
Treatment (Ptx vs GO-Ptx vs GO-HA-Ptx)	*** (p < 0.001)

Bonferroni post-tests

Ptx vs. GO-Ptx

Concentration (nM)	P value
40	P > 0.05
20	P > 0.05
10	P > 0.05
5	P > 0.05
2.5	P > 0.05
1.25	P > 0.05
0.625	P > 0.05

Ptx vs. GO-HA-Ptx

Concentration (nM)	P value
40	P > 0.05
20	P > 0.05
10	P > 0.05
5	P > 0.05
2.5	P > 0.05
1.25	P > 0.05
0.625	P > 0.05

GO-Ptx vs. GO-HA-Ptx

Concentration (nM)	P value
40	P > 0.05
20	P > 0.05
10	P > 0.05
5	P > 0.05
2.5	* - P < 0.05
1.25	P > 0.05
0.625	P > 0.05

Figure 7. Cytotoxicity of Ptx-loaded nanoparticulates. Varying concentrations of Ptx (either in a suspension form or on particulates) were added to MDA-MB-231 cells, and their effect on cell viability was determined. Cell viability measurements are normalized to control cultures of cells in the absence of any Ptx or particulates. Statistical analysis of data was performed, and significant differences were observed, which are reported in tables associated with the graph.

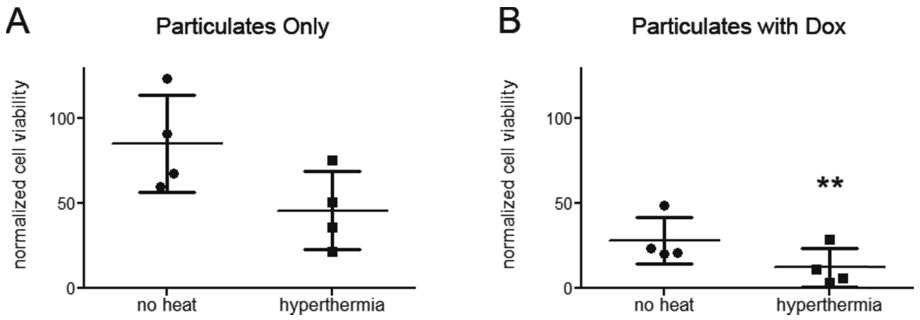

Figure 8. Cytotoxicity induced by combination of drug treatment and hyperthermia. GO-HA-iron oxide particulates (A) without or (B) with Dox were cultured with MDA-MB-231 cells and exposed to magnetic fields, and cell viability was measured. Cell viability measurements are normalized to control cultures of cells in the absence of particulates, drugs, and hyperthermia. Paired Student's *t*-test was performed to compare hyperthermia treatment to their respective no-heat controls. $^{**}p < 0.01$.

potential to be used in a number of biomedical applications, and we have showcased one such use for killing breast cancer cells.

EXPERIMENTAL SECTION

Synthesis of Graphene Oxide by Modified Hummers Methods. Graphene oxide (GO) was synthesized using the modified Hummers method followed by sonication.[31] Briefly, graphite flakes (Merck, USA), sodium nitrate, and potassium permanganate (SRL Chemicals, Mumbai, India) were mixed at a ratio of 2:1:6 in the presence of concentrated H_2SO_4 in an ice bath (at 0−5 °C). The reaction mixture was diluted by adding distilled water under vigorous stirring followed by addition of hydrogen peroxide (30%, v/v; Merck, India) to terminate the reaction. The resulting mixture was centrifuged at ∼3000*g* for 10 min, and the pellet was washed with 10% hydrochloric acid solution to remove the metal ions followed by repeated washing with distilled water to get the solution having pH 7. Purified GO was finely dispersed in distilled water and sonicated for 2−4 h to facilitate the synthesis of nanoparticulates.

Amination of Hyaluronic Acid. Hyaluronic acid (HA, SRL Chemicals, India) was reacted with ethylene diamine (EDA) to obtain free amine groups on HA that would enable a reaction with GO. Briefly, 8.8 mg of HA (M_w = 80−100 kDa) was first dissolved in 9 mL of 0.1 mM MES buffer at room temperature. Then, 5 mg of EDAC·HCl and 7 mg of NHS were added to enable activation of the carboxyl group. After 2 h of stirring, the pH of the solution was adjusted to ∼7.3 using 0.1 N sodium hydroxide solutions, and 20 μL of 1 mM cold EDA solution was added to initiate the modification of HA. After 4 h of reaction,

DOI: 10.1021/acsomega.9b00870
ACS Omega 2019, 4, 9284−9293

the mixture was kept for dialysis against excess deionized water for 24 h. The prepared HA-EDA was stored at 4 °C.

Hyaluronic Acid Functionalization of Graphene Oxide. To incorporate HA onto the graphene oxide nanoparticulates, the carboxyl group of GO and amine group of HA-EDA were conjugated using the aforementioned carbodiimide chemistry. Briefly, GO (1 mg/mL) and HA-EDA (0.1 mg/mL) were mixed with EDC (6 mg) and NHS (6 mg) in MES buffer (0.1 M, pH 5.4) at 37 °C under constant stirring for 8 h. The obtained product was first centrifuged at 16,000*g* for 10 min to collect the hyaluronic acid-grafted graphene oxide as a pellet and washed twice using deionized water. Finally, the redispersed solution was dialyzed against deionized water for 48 h. The prepared GO-HA particulate was stored at 4 °C.

Composite Preparation: Gelatin-Coated Fe_3O_4-Impregnated GO-HA. First, a coprecipitation method was followed to synthesize the iron oxide (Fe_3O_4) nanoparticle, where $FeCl_3$ and $FeSO_4{\cdot}7H_2O$ (2:1 molar ratio) were mixed under alkaline condition (NH_4OH/0.7 M NaOH). The product was centrifuged and washed twice with deionized water to remove the impurities. Then, it was dried and stored. In the second step, 5 mg of as-prepared Fe_3O_4 was added to 10 mL of gelatin solution (1.5 mg/mL in water), and the mixture was sonicated for 2 h. Next, it was centrifuged, and the supernatant was stored at 37 °C. In the final step, 5 mL of prepared gelatin-Fe_3O_4 was added dropwise to 5 mL of 1 mg/mL GO-HA solution and left under stirring condition at room temperature. After 12 h of incubation, the mixture was centrifuged and washed twice. Finally, the pellet was dried and stored for further analysis.

Characterization. UV−visible spectral analysis of GO, GO-HA, Doxorubicin (Dox, Merck), and paclitaxel (PTX, SRL Chemicals) solutions was done on a UV−visible spectrophotometer (NanoDrop 1000, ThermoFisher Scientific) with a resolution of 1 nm. Fourier transform infrared (FTIR) spectra of GO, HA, and GO-HA nanoparticles were recorded using a PerkinElmer FTIR spectrometer (model: L1860121, USA), scanning from 4000 to 500 cm^{-1} for 42 consecutive scans at room temperature. The hydrodynamic diameter and zeta potential values of the nanoparticulates were measured using a Zetasizer Nano ZS dynamic light-scattering instrument (Malvern, UK) at room temperature. The surface morphology of the particulates was determined using an atomic force microscope (NX-10 AFM, Park System, South Korea, along with XEI Software for imaging) in a tapping mode at room temperature. The interlayer spacings and diffraction patterns of graphite flakes, graphene oxide, and hyaluronic acid-conjugated graphene oxide were monitored using X-ray diffraction, filled with Rigaku filtered Cu Kα radiation operated at 40 KV and 30 mA over the range of $2\theta = 5°-90°$. The exfoliation of GO and GO-HA was observed using a transmission electron microscope (Titan THEMIS, 300 KeV). The structural order of the particulates was investigated using a Raman microscope (532 nm laser, LabRAM HR). Elemental composition was assessed using X-ray photoelectron spectroscopy (Al-monochromatic radiation, 1486.6 eV, model: Kratos Axis Ultra DLD).

Drug Loading and Release Study. To load Dox or paclitaxel (Ptx, SRL Chemicals) onto particulates, freshly prepared 500 μM drug solution (in DMSO) was added to 200 μL aqueous suspension of GO or GO-HA (0.5 mg/mL) and placed on a spinning rotor (25 rpm) at room temperature in the absence of light. After overnight incubation, drug loaded systems were centrifuged at ∼16,900*g* for 10 min at 4 °C. The pellet was washed twice in sterilized 1× PBS to remove the loosely bound drug molecules. The final product was suspended in 200 μL 1× PBS and stored at 4 °C. The supernatant from centrifugation was collected, and the amount of drug present was assessed [absorbance at 488 nm (Dox) and 231 nm (Ptx)] using the free drug standard curve. The drug adsorption efficiency (AE; also loading efficiency) was determined as below

$$\mathrm{AE}(\%) = \frac{(\text{initial concn of Dox/Ptx} - \text{concn of Dox/Ptx in supernatant})}{\text{initial concn of Dox/Ptx}} \times 100$$

In vitro release studies were performed in solutions of pH 5.5 (sodium acetate buffer) and pH 7.4 (phosphate buffered saline) at 37 °C under shaking condition. At specified time intervals, Dox-loaded particulates were centrifuged at 16900*g* for 10 min, and 160 μL of supernatant was collected at each time point, followed by the addition of 160 μL of respective fresh sodium acetate or PBS solution. Finally, the absorbance of the supernatant was measured using the NanoDrop method at 488 nm, and the percentage of the cumulative drug was calculated using the following relation

$$\text{cumulative release (concn)} = \left(\frac{\text{vol. of sample withdrawn}}{\text{total vol. of release}} \times C_{t-1}\right) + C_t$$

where C_t and C_{t-1} are concentrations of the drug measured at times t and $t-1$.

Cell Toxicity Assays. The efficacy of drug-loaded nanoparticulates and the intrinsic toxicity of the particulates without the drug were determined by culturing these particulates with $CD44^-$ BT-474 or $CD44^+$ MDA-MB-231 breast cancer cell lines and performing a standard MTT assay. For toxicity studies, both the cell lines (5×10^3) in DMEM (10% FBS and 1% antibiotics) were seeded in individual wells of a 96-well culture plate and incubated at 37 °C (and in the presence of 5% CO_2) for 12 h. Varying concentrations of nanoparticulates (100−6.25 μg/mL) were added to the cell pates, and these mixtures were incubated for another 24 h. Finally, the culture plates were washed twice using sterilized 1× PBS solution and incubated with 200 μL (0.5 mg/mL) of MTT solution in the dark at room temperature for 3 h. Following the addition of DMSO, the absorbance was measured at 570 nm according to the method described by Qin et al.[32] To investigate drug (Dox or Ptx)-mediated cytotoxicity, varying concentrations of free drug or drug-loaded particulates (equivalent concentration of the drug) were incubated with the two different cell lines for 48 h. Then, the individual wells were washed twice with sterile PBS and incubated with 200 μL MTT solution (0.5 mg/mL) in the dark at room temperature for 3 h, followed by measurement of absorbance at 570 nm.

Hyperthermia. Magnetic hyperthermia experiments were performed in an EASYHEAT induction system (4.2 kW Ambrell, USA). To measure the change in temperature, the experimental sample (with or without magnetic nanoparticles and with or without cells) was placed into the system and exposed to an AC magnetic field at 235 kHz under 400.5 A (RF coil current) for 10 min. Temperature change was recorded, and if the samples contained cells, the sample was retrieved and placed in a culture.

In Vitro Degradation of Graphene Oxide Nanomaterials. To investigate the effect of immune cells on the degradation of graphene oxide nanomaterials, the particulates were cultured with RAW 264.7 (macrophage) cells, and confocal Raman spectral analysis was performed on the supernatant. For these studies, initially, cells (20×10^3) were cultured in 96-well plates

DOI: 10.1021/acsomega.9b00870
ACS Omega 2019, 4, 9284−9293

in 200 μL of DMEM media for 12 h. Next, varying concentrations of particulates (0.5, 0.05, 0.01, and 0.001 mg/mL) were incubated for 24 h with the cells. The supernatant from these cultures were collected and centrifuged at 10,000*g* for 10 min. The supernatant from centrifugation was first dialyzed against MQ water for 48 h and analyzed.

Statistical Analysis. In studies involving cells, three independent repeats were performed for each experiment, and within each experiment, the assays were usually performed in duplicates. Data is reported as the mean of each independent repeat ± standard deviations (SD). Repeated measured two-way ANOVA followed by the Bonferroni post-hoc test was used to statistically compare data, except for the hyperthermia studies where Student's paired *t*-test was used for statistical comparisons.

■ ASSOCIATED CONTENT

Supporting Information

The Supporting Information is available free of charge on the ACS Publications website at DOI: 10.1021/acsomega.9b00870.

The following data is available as supporting information. Transmission electron micrographs along with carbon and oxygen elemental mapping of GO and GO-HA; UV-Vis and FTIR spectroscopies of Ptx- and Dox-loaded nanoparticulates; fluorescence microscopy images to determine the uptake of GO and GO-HA by MDA-MB-231 cells; X-ray photoelectron spectroscopy of the composite and elemental analysis confirming iron oxide nanoparticle embedding on GO-HA; VSM magnetic hysteresis analysis showing the magnetic property of the composite system and magnetic hyperthermia measurements showing the composite system at various concentrations; and Raman spectroscopy assessing the degradation of nanoparticulates when cultured with RAW macrophage cells (PDF)

■ AUTHOR INFORMATION

Corresponding Author

*E-mail: siddharth@iisc.ac.in.

ORCID

Shilpee Jain: 0000-0002-2909-9476

Siddharth Jhunjhunwala: 0000-0001-8046-2288

Notes

The authors declare no competing financial interest.

■ ACKNOWLEDGMENTS

This work was supported by the Science and Engineering Board, Department of Science and Technology, Government of India, national postdoctoral fellowship to N.P. (PDF/2016/001685) and Ramanujan Fellowship (SB/S2/RJN-135/2015) to S. Jhunjhunwala. S. Jhunjhunwala is in receipt of the R.I. Mazumdar young investigator award, which partly funded this work. Authors sincerely acknowledge Punarbasu Roy for his technical support in the experiments and analysis.

■ REFERENCES

(1) Goenka, S.; Sant, V.; Sant, S. Graphene-Based Nanomaterials for Drug Delivery and Tissue Engineering. *J. Controlled Release* **2014**, *173*, 75−88.

(2) Ghosal, K.; Sarkar, K. Biomedical Applications of Graphene Nanomaterials and Beyond. *ACS Biomater. Sci. Eng.* **2018**, *4*, 2653−2703.

(3) Tadyszak, K.; Wychowaniec, J.; Litowczenko, J. Biomedical Applications of Graphene-Based Structures. *Nanomaterials* **2018**, *8*, 944.

(4) Shim, G.; Kim, M.-G.; Park, J. Y.; Oh, Y.-K. Graphene-Based Nanosheets for Delivery of Chemotherapeutics and Biological Drugs. *Adv. Drug Delivery Rev.* **2016**, *105*, 205−227.

(5) de Melo-Diogo, D.; Lima-Sousa, R.; Alves, C. G.; Costa, E. C.; Louro, R. O.; Correia, I. J. Functionalization of Graphene Family Nanomaterials for Application in Cancer Therapy. *Colloids Surf., B* **2018**, *171*, 260−275.

(6) Tripodo, G.; Trapani, A.; Torre, M. L.; Giammona, G.; Trapani, G.; Mandracchia, D. Hyaluronic Acid and Its Derivatives in Drug Delivery and Imaging: Recent Advances and Challenges. *Eur. J. Pharm. Biopharm.* **2015**, *97*, 400−416.

(7) Senbanjo, L. T.; Chellaiah, M. A. CD44: A Multifunctional Cell Surface Adhesion Receptor Is a Regulator of Progression and Metastasis of Cancer Cells. *Front. Cell Dev. Biol.* **2017**, *5*, 18.

(8) Wu, H.; Shi, H.; Wang, Y.; Jia, X.; Tang, C.; Zhang, J.; Yang, S. Hyaluronic Acid Conjugated Graphene Oxide for Targeted Drug Delivery. *Carbon* **2014**, *69*, 379−389.

(9) Song, E.; Han, W.; Li, C.; Cheng, D.; Li, L.; Liu, L.; Zhu, G.; Song, Y.; Tan, W. Hyaluronic Acid-Decorated Graphene Oxide Nanohybrids as Nanocarriers for Targeted and pH-Responsive Anticancer Drug Delivery. *ACS Appl. Mater. Interfaces* **2014**, *6*, 11882−11890.

(10) Jung, H. S.; Lee, M.-Y.; Kong, W. H.; Do, I. H.; Hahn, S. K. Nano Graphene Oxide−hyaluronic Acid Conjugate for Target Specific Cancer Drug Delivery. *RSC Adv.* **2014**, *4*, 14197.

(11) Li, F.; Park, S.-J.; Ling, D.; Park, W.; Han, J. Y.; Na, K.; Char, K. Hyaluronic Acid-Conjugated Graphene Oxide/Photosensitizer Nanohybrids for Cancer Targeted Photodynamic Therapy. *J. Mater. Chem. B* **2013**, *1*, 1678.

(12) Yin, T.; Liu, J.; Zhao, Z.; Zhao, Y.; Dong, L.; Yang, M.; Zhou, J.; Huo, M. Redox Sensitive Hyaluronic Acid-Decorated Graphene Oxide for Photothermally Controlled Tumor-Cytoplasm-Selective Rapid Drug Delivery. *Adv. Funct. Mater.* **2017**, *27*, 1604620.

(13) Jiang, W.; Mo, F.; Jin, X.; Chen, L.; Xu, L. J.; Guo, L.; Fu, F. Tumor-Targeting Photothermal Heating-Responsive Nanoplatform Based on Reduced Graphene Oxide/Mesoporous Silica/Hyaluronic Acid Nanocomposite for Enhanced Photodynamic Therapy. *Adv. Mater. Interfaces* **2017**, *4*, 1700425.

(14) Lima-Sousa, R.; de Melo-Diogo, D.; Alves, C. G.; Costa, E. C.; Ferreira, P.; Louro, R. O.; Correia, I. J. Hyaluronic Acid Functionalized Green Reduced Graphene Oxide for Targeted Cancer Photothermal Therapy. *Carbohydr. Polym.* **2018**, *200*, 93−99.

(15) Mallick, A.; Mahapatra, A. S.; Mitra, A.; Greneche, J. M.; Ningthoujam, R. S.; Chakrabarti, P. K. Magnetic Properties and Bio-Medical Applications in Hyperthermia of Lithium Zinc Ferrite Nanoparticles Integrated with Reduced Graphene Oxide. *J. Appl. Phys.* **2018**, *123*, No. 055103.

(16) Kolosnjaj-Tabi, J.; Wilhelm, C. Magnetic Nanoparticles in Cancer Therapy: How Can Thermal Approaches Help? *Nanomedicine* **2017**, *12*, 573−575.

(17) Saeed, M.; Ren, W.; Wu, A. Therapeutic Applications of Iron Oxide Based Nanoparticles in Cancer: Basic Concepts and Recent Advances. *Biomater. Sci.* **2018**, *6*, 708−725.

(18) Chang, D.; Lim, M.; Goos, J. A. C. M.; Qiao, R.; Ng, Y. Y.; Mansfeld, F. M.; Jackson, M.; Davis, T. P.; Kavallaris, M. Biologically Targeted Magnetic Hyperthermia: Potential and Limitations. *Front. Pharmacol.* **2018**, *9*, 831.

(19) Tiwari, P.; Agarwal, S.; Srivastava, S.; Jain, S. The Combined Effect of Thermal and Chemotherapy on HeLa Cells Using Magnetically Actuated Smart Textured Fibrous System. *J. Biomed. Mater. Res. B Appl. Biomater.* **2018**, *106*, 40−51.

(20) Eda, G.; Chhowalla, M. Chemically Derived Graphene Oxide: Towards Large-Area Thin-Film Electronics and Optoelectronics. *Adv. Mater.* **2010**, *22*, 2392−2415.

(21) Wu, J.-B.; Lin, M.-L.; Cong, X.; Liu, H.-N.; Tan, P.-H. Raman Spectroscopy of Graphene-Based Materials and Its Applications in Related Devices. *Chem. Soc. Rev.* **2018**, *47*, 1822−1873.

DOI: 10.1021/acsomega.9b00870
ACS Omega 2019, 4, 9284−9293

(22) Jasim, D. A.; Lozano, N.; Kostarelos, K. Synthesis of Few-Layered, High-Purity Graphene Oxide Sheets from Different Graphite Sources for Biology. *2D Mater.* **2016**, *3*, No. 014006.
(23) Drewniak, S.; Muzyka, R.; Stolarczyk, A.; Pustelny, T.; Kotyczka-Morańska, M.; Setkiewicz, M. Studies of Reduced Graphene Oxide and Graphite Oxide in the Aspect of Their Possible Application in Gas Sensors. *Sensors* **2016**, *16*, 103.
(24) He, H.; Hu, Y.; Chen, S.; Zhuang, L.; Ma, B.; Wu, Q. Preparation and Properties of A Hyperbranch-Structured Polyamine Adsorbent for Carbon Dioxide Capture. *Sci. Rep.* **2017**, *7*, 3913.
(25) Jin, J.; Krishnamachary, B.; Mironchik, Y.; Kobayashi, H.; Bhujwalla, Z. M. Phototheranostics of CD44-Positive Cell Populations in Triple Negative Breast Cancer. *Sci. Rep.* **2016**, *6*, 27871.
(26) Zhou, J.; Giannakakou, P. Targeting Microtubules for Cancer Chemotherapy. *Curr. Med. Chem.: Anti-Cancer Agents* **2005**, *5*, 65−71.
(27) Sydlik, S. A.; Jhunjhunwala, S.; Webber, M. J.; Anderson, D. G.; Langer, R. In Vivo Compatibility of Graphene Oxide with Differing Oxidation States. *ACS Nano* **2015**, *9*, 3866−3874.
(28) Mukherjee, S. P.; Gliga, A. R.; Lazzaretto, B.; Brandner, B.; Fielden, M.; Vogt, C.; Newman, L.; Rodrigues, A. F.; Shao, W.; Fournier, P. M.; et al. Graphene Oxide Is Degraded by Neutrophils and the Degradation Products Are Non-Genotoxic. *Nanoscale* **2018**, *10*, 1180−1188.
(29) Kurapati, R.; Mukherjee, S. P.; Martín, C.; Bepete, G.; Vázquez, E.; Pénicaud, A.; Fadeel, B.; Bianco, A. Degradation of Single-Layer and Few-Layer Graphene by Neutrophil Myeloperoxidase. *Angew. Chem., Int. Ed.* **2018**, *57*, 11722−11727.
(30) Kurapati, R.; Bonachera, F.; Russier, J.; Sureshbabu, A. R.; Ménard-Moyon, C.; Kostarelos, K.; Bianco, A. Covalent Chemical Functionalization Enhances the Biodegradation of Graphene Oxide. *2D Mater.* **2017**, *5*, No. 015020.
(31) Ojha, K.; Anjaneyulu, O.; Ganguli, A. K. Graphene-Based Hybrid Materials: Synthetic Approaches and Properties. *Curr. Sci.* **2014**, *107*, 397−418.
(32) Qin, X. C.; Guo, Z. Y.; Liu, Z. M.; Zhang, W.; Wan, M. M.; Yang, B. W. Folic Acid-Conjugated Graphene Oxide for Cancer Targeted Chemo-Photothermal Therapy. *J. Photochem. Photobiol., B* **2013**, *120*, 156−162.

DOI: 10.1021/acsomega.9b00870
ACS Omega 2019, 4, 9284−9293